American Mineralogist, Volume 100, pages 1736–1743, 2015

SPINELS RENAISSANCE: THE PAST, PRESENT, AND FUTURE OF THOSE UBIQUITOUS MINERALS AND MATERIALS

New structure of high-pressure body-centered orthorhombic Fe_2SiO_4†

Takamitsu Yamanaka[1,]*, Atsushi Kyono[1,3], Yuki Nakamoto[1,4], Svetlana Kharlamova[1], Viktor V. Struzhkin[1], Stephen A. Gramsch[1], Ho-kwang Mao[1,2] and Russell J. Hemley[1]

[1]Geophysical Laboratory, Carnegie Institution of Washington, Washington, D.C. 20015, U.S.A.
[2]High Pressure Collaborative Access Team, Geophysical Laboratory, Carnegie Institution of Washington, Argonne, Illinois 60439, U.S.A.
[3]Division of Earth Evolution Sciences, Graduate School of Life and Environment Sciences, University of Tsukuba, Tsukuba Ibaraki, 305-8572, Japan
[4]Center for Quantum Science and Technology Under Extreme Conditions, Osaka University, Toyonaka Osaka, 560-8531, Japan

Abstract

A structural change in Fe_2SiO_4 spinel (ringwoodite) has been found by synchrotron powder diffraction study and the structure of a new high-pressure phase was determined by Monte-Carlo simulation method and Rietveld profile fitting of X-ray diffraction data up to 64 GPa at ambient temperature. A transition from the cubic spinel structure to a body centered orthorhombic phase (I-Fe_2SiO_4) with space group *Imma* and $Z = 4$ was observed at approximately 34 GPa. The structure of I-Fe_2SiO_4 has two crystallographically independent FeO_6 octahedra. Iron resides in two different sites of sixfold coordination: Fe1 and Fe2, which are arranged in layers parallel to (101) and (011) and are very similar to the layers of FeO_6 octahedra in the spinel structure. Silicon is located in the sixfold coordination in I-Fe_2SiO_4. The transformation to the new high-pressure phase is reversible under decompression at ambient temperature. A martensitic transformation of each slab of the spinel structure with translation vector $<\overrightarrow{1/8}\ \overrightarrow{1/8}\ \overrightarrow{1/8}>$ generates the I-Fe_2SiO_4 structure. Laser heating of I-Fe_2SiO_4 at 1500 K results in a decomposition of the material to rhombohedral FeO and SiO_2 stishovite.

Fe$K\beta$ X-ray emission measurements at high pressure up to 65 GPa show that the transition from a high spin (HS) to an intermediate spin (IS) state begins at 17 GPa in the spinel phase. The IS electron spin state is gradually enhanced with pressure. The Fe^{2+} ion at the octahedral site changes the ion radius under compression at the low spin, which results in the changes of the lattice parameter and the deformation of the octahedra of the spinel structure. The compression curve of the lattice parameter of the spinel is discontinuous at ~20 GPa. The spin transition induces an isostructural change.

Keywords: New high-pressure structure, Fe_2SiO_4 ringwoodite, X-ray emission spectra, spin transition, martensitic transition

Introduction

A great deal of attention has been paid to the high-pressure structural transitions of the many spinel phases present in the Earth's crust due to their geophysical importance (Akimoto and Fujisawa 1967; Bassett and Ming 1972; Ito and Takahashi 1987; Irifune et al. 1998). One of the major minerals in the crust, $(Mg,Fe)_2SiO_4$ olivine (α-phase), transforms to wadsleyite (β-phase, modified spinel) and further to ringwoodite (γ-phase, spinel). These transitions were proposed for the origin of the seismic discontinuity of the transition zone from 410 to 660 km depth (Ringwood and Irifune 1988). These high-pressure transformations have been studied from various viewpoints, including the electronic and elastic properties of participating phases (Kiefer et al. 1997; Li et al. 2007) and continue to provide significant information for seismic interpretation (Leven et al. 1981; Burnley et al. 1991; Shim et al. 2001).

Recently, the Fe_2SiO_4 phase with spinel structure was found in meteorite, and silicate spinels of transition elements are investigated for their influence on the magnetic and electrical properties of the Earth's crust and mantle. Their phase stabilities and structures under high-pressure and high-temperature conditions have been intensively studied. Phase relations in the Mg_2SiO_4-Fe_2SiO_4 ringwoodite solid solution system have been investigated in numerous high-pressure studies (Katsura and Ito 1989; Ito and Takahashi 1989; Fei et al. 1999; Matsuzaka et al. 2000). Mechanisms for the polymorphic transformations of the α, β, and γ phases of (Mg, have been discussed in terms of the observation of dislocations by TEM (Price et al. 1982; Madon and Poirier 1983). Structures of silicate spinels M_2SiO_4 (M = Mg, Fe, Co, Ni) have been refined from X-ray diffraction data at ambient conditions (Yagi et al. 1974; Morimoto et al. 1970, 1974; Ma 1975; Marumo et al. 1974, 1977). (1981). End-member of ringwoodite solid solution, Fe_2SiO_4, undergoes transitions at 6.4 GPa at 1700 °C (Yagi et al. 1987). Further experimental studies have been undertaken by Fei et al. (1991) and Matsuzaka (2000).

Significant work is also focused on the physical properties of iron-bearing spinels to understand their strong electronic

* E-mail: tyamanaka@ciw.edu
† Special collection papers can be found on GSW at http://ammin.geoscienceworld.org/site/misc/specialissuelist.xhtml.

0003-004X/15/0809–1736$05.00/DOI: http://dx.doi.org/10.2138/am-2015-4744

correlations as manifested in charge transfer, electron hopping and the Jahn-Teller effect, in particular through magnetic and electrical conductivity measurements and Raman spectroscopy (Ohtaka et al. 1997; Xu et al. 1998; Woodland and Angel 2000; Woodland et al. 2010; Yamanaka and Okita 2001; Yamanaka et al. 2001; Kontny et al. 2004).

Recently, at pressures above 30 GPa and ambient temperature, a pseudo-rhombohedral phase of Fe_2SiO_4 was proposed as high-pressure phase by powder diffraction and Mössbauer spectroscopy measurements (Greenberg et al. 2011). It has been reported that the spinel phase of Fe_2SiO_4 decomposes to FeO (wüstite) and SiO_2 (stishovite) at higher pressures (Katsura and Ito 1989; Ito and Takahashi 1989), because the Si atom is too small make any of the post-spinel phases stable at high pressure (Ito and Takahashi 1989).

Single-crystal structure analyses of Fe_2SiO_4 spinel have been carried out using a diamond-anvil cell up to 8.9 GPa by Hazen (1993) and up to 10.2 GPa by Nestola et al. (2011). Lattice dynamics and thermodynamic properties of antiferromagnetic Fe_2SiO_4 spinel were determined using phonon dispersion curves from density functional theory at pressures up to 20 GPa (Jing and Guo 2004; Derzsi et al. 2011).

Electronic spin transitions attributed to change from the high-spin (HS) to low-spin (LS) states in transition metals, particularly iron, have been increasingly used to understand anomalies in the properties of oxides and silicates at high pressure. X-ray emission spectroscopy (XES), carried out using a synchrotron source and DAC techniques, is a method for probing the spin state of iron at high pressures (Badro et al. 1999; Mattila et al. 2007; Li et al. 2004; Lin et al. 2005). The spin state change of Fe^{2+} in the octahedral site is accelerated at higher pressures.

In the present experiment, the details of the structural transformation of Fe_2SiO_4 ringwoodite due to an electronic spin transition were elucidated by X-ray diffraction and X-ray emission measurements up to 64 GPa at ambient temperature. A new high-pressure phase was determined to have a body-centered orthorhombic structure in space group *Imma* (z = 4) rather than rhombohedral $R\overline{3}m$, which was previously proposed by Greenberg et al. (2011). The correlation between the structural transition and the spin state is also investigated by XES experiment.

Experimental methods

Synchrotron X-ray diffraction and structure analysis

Fe_2SiO_4 spinel was prepared using a multi-anvil high-pressure apparatus. A mixture of Fe_2O_3 and SiO_2 was heated at 1500 °C for 5 h under an atmosphere of CO_2 and H_2 with a mixing ratio of 1/1. The quenched sample was confirmed to be fayalite Fe_2SiO_4, which then served as the starting material for a high-pressure synthesis of the spinel phase. The powdered fayalite was placed directly into a cylindrical graphite heater that was set at the center of an octahedral pressure medium. The synthesis conditions were 8 GPa and 1400 °C for 1 h, employing the Kawai-type multi-anvil apparatus installed at ISEI, Okayama University. The graphite heater prevented oxidation to ferric iron. The product was confirmed to be single-phase spinel by electron microprobe analyzer and powder X-ray diffraction.

Angle-dispersive powder X-ray diffraction was carried out using synchrotron radiation with wavelength 0.4262 Å at beamline 16-BM-D at the Advanced Photon Source (APS), Argonne National Laboratory. A highly focused X-ray beam with 2 mm in diameter was aligned with the center of the sample chamber in the diamond-anvil cell (DAC). The diffraction patterns of the samples were recorded with an imaging plate (MAR-345) and processed with FIT2D software (http://www.esrf.fr/computing/scientific/FIT2D/). The detector tilting and the distance between the sample and detector were calibrated against the known lattice parameters of CeO_2. The lattice parameters of the samples were determined by fitting the observed diffraction peaks. A symmetric diamond-anvil cell (DAC) was prepared with diamonds having culet and 450 in diameter. The sample chamber consisted of a hole drilled in a rhenium gasket with initial thickness of 200 μm and to 60 μm. The fine powder spinel sample, together with a ruby chip for a pressure marker, was loaded in the sample chamber. Ne served as the pressure medium and was loaded into the cell using a gas loading apparatus. Pressure was determined by the ruby luminescence method (Piermarini et al. 1975; Mao et al. 1986). An off-line laser heating system in the double-sided configuration, and consisting of a laser along with associated optics, was used to heat the sample. The temperature during laser heating was ~1500 K, which was determined using spectral radiometry based on the Planck radiation function.

For the diffraction patterns of two-phase mixture over 39 GPa, the lattice parameters were obtained using the DICVOL, indexing routine (Boultif and Louer 2004), with about 12 reasonable and strong reflections in range $2\theta = 4–20°$. Subsequently, a Monte-Carlo method was applied to find candidates for the high-pressure structure using the diffraction intensities with fixed lattice parameters as determined by DICVOL. Rietveld profile fitting was then performed with the program RIETAN-2000 (Izumi and Ikeda 2000) using the initial model observed from the Monte-Carlo simulation. To fit the data, the background intensity distribution was first adjusted for the refinement. Lattice parameters, atomic positional coordinates and temperature factors were treated as variable parameters. Subsequently, profile parameters (full-width at half maximum, asymmetry parameters and angular decay parameter) were varied in the refinement. A preferred orientation correction was made considering the spinel cleavage habit. Finally a full matrix, least-squares refinement was conducted.

X-ray emission spectroscopy (XES)

X-ray emission spectra (XES) measurements on Fe_2SiO_4 were carried out up to 65 GPa at ambient temperature at beamline 16-ID-D APS. The spin state of ferrous iron is characterized by the appearance of a satellite emission peak located in the lower energy region of the main emission peak which is a result of the 3*p*–3*d* core–hole exchange. The experimental setup and specifications of the apparatus are described in a previous report (Yamanaka et al. 2013). A panoramic DAC, with a configuration similar to that used in the synchrotron diffraction experiments was prepared for the XES measurements, except that a Be gasket was used instead of an Re gasket.

We applied the variation of the spin state through the integrated absolute values of the difference spectra (IAD) (Vanko et al. 2006). The high-spin (HS) and low-spin (LS) spectral functions are normalized to unit area at integration. The IAD value for the complete spin transition can be given as $IAD_{HL} = \int|h(E) - l(E)|dE$. A spectrum in the transition region is a superposition of those of the two spin states, thus it can be expressed as $s = \gamma_{HS} h + (1 - \gamma_{HS})l$, where γ_{HS} is the high-spin fraction. Its difference from the low-spin reference l is $s - l = \gamma_{HS}(h - l)$. The integral of its absolute value is

$$IAD(s) = \int|s(E) - l(E)|dE = \gamma_{HS} IAD_{HL}.$$

The IAD is proportional to a fraction of the high spin and is a good indicator of the amount of the transition.

Results

Compression of the lattice parameter Fe_2SiO_4 spinel and structure transition

Selected powder diffraction patterns obtained at increasing pressures up to 54.6 GPa at ambient temperature are shown in Figure 1. Up to 34.8 GPa, the patterns show a single phase with the spinel structure. A new pattern, different from that of the spinel phase, was observed above 38.8 GPa, although the spinel pattern was detected even at 54.6 GPa as a residual phase.

In Fe_2SiO_4 spinel, Si is located in the tetrahedral site and Fe on octahedral sites, resulting in a normal spinel with space group $Fd\overline{3}m$. Only two parameters, the oxygen positional parameter u and the lattice parameter a, are variables in the structure refinement. The lattice parameter and density as determined from the Rietveld refinement are presented in Table 1 in which those data

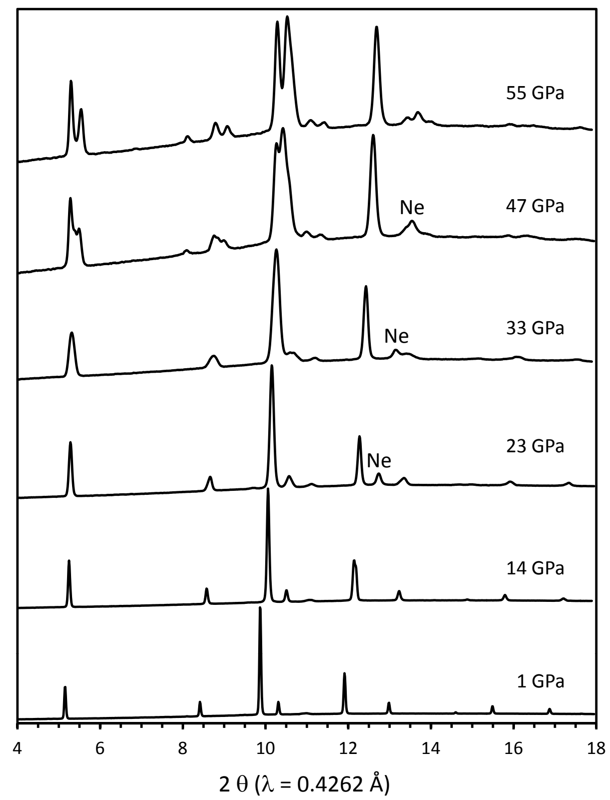

FIGURE 1. Selected X-ray diffraction patterns of Fe_2SiO_4 taken with increasing pressure at ambient temperature. The high-pressure phase was found above 38.8 GPa and observed up to 56.6 GPa.

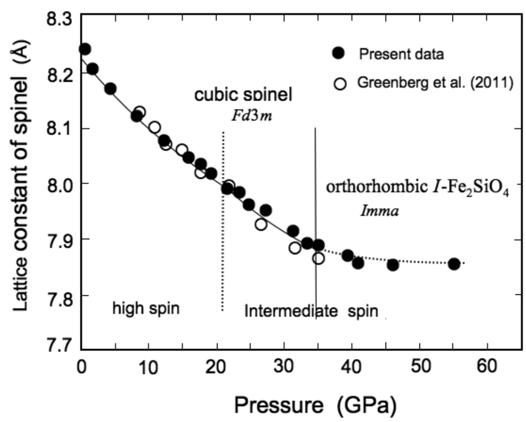

FIGURE 2. There are two distinct compression regimes indicating the boundary at about 20 GPa. This behavior is a little higher pressure than the HS-to-IS transition of 17 GPa observed by XES. The data of Greenberg et al. (2011) are also presented. The dotted curve represents the lattice parameter of the residual spinel coexist with I-Fe_2SiO_4. The observed error is smaller than the data point.

TABLE 1. Lattice constant of Fe_2SiO_4 spinel

P (GPa)	LC (Å)
Spinel stable region	
0.0001	8.2374(4)
1.2	8.2156(8)
3.7	8.1783(9)
4.0	8.1756(8)
7.8	8.1325(8)
9.1	8.1140(8)
11.5	8.0905(8)
13.3	8.0759(9)
15.4	8.057(1)
17.3	8.044(1)
18.8	8.028(1)
20.3	8.013(1)
22.3	7.996(1)
23.1	7.990(1)
24.2	7.976(2)
27.2	7.951(2)
31.0	7.916(2)
32.9	7.895(2)
34.8	7.889(3)
Two-phase mixture metastable spinel	
38.8	7.879(4)
39.2	7.855(4)
44.6	7.756(2)
54.6	7.730(2)

Note: Spinel phase is found at pressures above the transition pressure of 38.8 GPa and coexists with the high-pressure phase of I-Fe_2SiO_4.

of the residual spinels over 38.8 GPa are also presented. The variation in the lattice parameters of spinel phase with pressure is illustrated in Figure 2. The parameter shows two distinct regimes of compression behavior, one in a lower pressure region between ambient pressure and 20 GPa, and another above the pressure. The Si-O and Fe-O distances are presented in Table 2. The Si-O and Fe-O distances and the volume of tetrahedron (SiO_4) and octahedron (FeO_6) are calculated from the Rietveld analysis. The variations of the volume ratios of these sites R(SiO_4) and R(FeO_6) with pressure are shown in Figure 3. The bulk modulus was calculated using the third-order (BM) equation of state (Birch 1947). In the lower pressure region between ambient pressure and 20 GPa, the bulk modulus is $K_0 = 177(10)$ GPa and $K_0' = 8.8(1.9)$, while in the high-pressure region between 20 and 54.6 GPa, $K_0 = 209(8)$ GPa and $K_0' = 3.8(0.5)$. Overall data all through pressures are $K_0 = 200(9)$ GPa and $K_0' = 4.3(7)$. These data are similar to the previous data: $K_0 = 201(8)$ GPa, $K_0' = 3.7(7)$ (Greenberg et al. 2011) and $K_0 = 204.5(7)$ GPa, $K_0' = 4.3(3)$ (Liu et al. 2008), and $K_0 = 202(4)$ GPa, $K_0' = 4$ (Armentrout and Kavner 2011).

Diffraction patterns obtained under decompression from 54.6 GPa down to 31.0 GPa are shown in Figure 4, and reveal the back-transformation from the high-pressure phase to the spinel phase, indicating a reversible transition. After the back-transformation, the spinel phase was heated to 1500 K, resulting in a decrease in pressure from 33 to 31 GPa. The diffraction pattern taken at 31 GPa shows partial decomposition of the spinel to rhombohedral FeO and SiO_2 stishovite together with residual spinel. It is probable that a longer heating period would enhance this decomposition. The recovered sample was again compressed to 55 GPa at ambient temperature, and the residual spinel transformed again to the high-pressure phase. The decomposition process confirmed the disproportionation of Fe_2SiO_4 to 2FeO+SiO_2, reported by Bassett and Ming (1972).

Orthorhombic high-pressure phase of Fe_2SiO_4

Rietveld profile fitting analysis of the diffraction patterns taken at 44.6 and 54.6 GPa at ambient temperature indicate a two-phase mixture consisting of the new high-pressure phase and the residual spinel phase. The pattern at 64 GPa confirms only high-pressure single phase without spinel phase. Greenberg et al. (2011) proposed a pseudo-rhombohedral phase at pressures above 30 GPa at ambient temperature from X-ray diffraction and Mössbauer data. In their structure analysis, the residual spinel phase was not considered in the Rietveld refinement and provided a fit to the rhombohedral $R\overline{3}m$ structure. Several peaks in the

TABLE 2. Bond distance and site volume of spinel phase under pressure

P (GPa)	Cell const. (Å)	*V* (Å^3)	u parameter	d(Si-O) (Å)	d(Fe-O) (Å)	*V* (SiO_4) (Å^3)	*V* (FeO_6) (Å^3)
0.0001	8.2374(4)	558.95(6)	0.3659(2)	1.654(7)	2.137(7)	2.321(2)	12.914(2)
1.2	8.2156(8)	554.52(7)	0.3661(2)	1.652(6)	2.130(6)	2.314(4)	12.784(3)
4.0	8.1756(8)	546.46(8)	0.3666(2)	1.652(6)	2.116(6)	2.269(2)	12.558(2)
9.1	8.1140(8)	534.20(7)	0.3673(2)	1.649(7)	2.093(6)	2.299(3)	12.156(3)
13.3	8.0759(5)	526.71(5)	0.3673(8)	1.641(5)	2.083(5)	2.267(1)	11.986(1)
17.3	8.044(1)	520.5(2)	0.3678(9)	1.641(17)	2.071(17)	2.269(9)	11.779(9)
23.1	7.990(1)	510.0(2)	0.3692(11)	1.650(18)	2.045(18)	2.304(12)	11.368(13)
32.9	7.895(3)	492.1(1)	0.3700(11)	1.641(13)	2.014(13)	2.268(12)	10.868(13)
34.8	7.889(3)	490.9(1)	0.3702(13)	1.642(12)	2.011(12)	2.274(22)	10.818(23)
			Metastable spinel above the transition pressure				
38.8	7.879(4)	489.1(1)	0.3705(25)	1.644(17)	2.006(17)	2.272(23)	10.74(23)
39.2	7.855(4)	484.7(1)	0.3711(22)	1.648(16)	1.995(16)	2.295(23)	10.57(23)
44.6	7.756(2)	466.6(3)	0.3707(15)	1.622(12)	1.973(12)	2.188(16)	10.22(16)
54.6	7.730(2)	461.9(2)	0.3708(11)	1.617(10)	1.966(10)	2.171(14)	10.11(14)

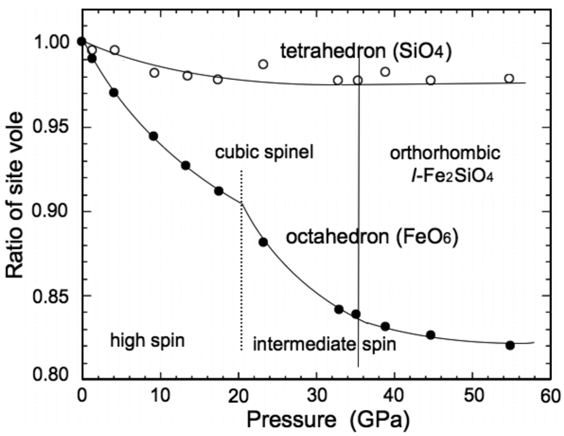

FIGURE 3. Average bond length ratio of tetrahedral and octahedral sites of Fe_2SiO_4 spinel. Bond lengths were obtained from the Rietveld profile fitting method. Error is smaller than the symbol mark. The Fe-O bond length in the octahedral site confirms the two different compression regimes at 20 GPa.

pattern, however, were not indexed or poorly fitted, as shown in Figure 5. A fit of the data obtained at 44.6 GPa to the rhombohedral structure does not result in a satisfactory refinement. On the other hand, a mixture of the orthorhombic high-pressure phase and spinel fits the 54.6 GPa data quite well (Fig. 6). The diffraction pattern corresponding only to the high-pressure phase was observed at 64 GPa (Fig. 7 and CIF[1] in the supplement file).

Rietveld analysis of the high-pressure diffraction data confirms that the new phase has a body-centered orthorhombic structure with space group symmetry of *Imma* and $Z = 4$. Hereafter the new phase is referred to as *I*-Fe_2SiO_4. Iron resides in two different sites of sixfold coordination: Fe1 with site symmetry of $2/m$ ($4b$) and Fe2 with site symmetry of $2/m$ ($4c$), where the letter in the parentheses is Wyckoff notation. These octahedra create layers parallel to (101) and (011) planes, and they are very similar to the octahedral layers that form (111) and ($1\bar{1}1$) planes of the spinel structure. The Fe octahedra in the spinel structure split two different F1 and Fe2 octahedra in the *I*-Fe_2SiO_4 structure. And the

[1] Deposit item AM-15-84744, CIF. Deposit items are stored on the MSA web site and available via the *American Mineralogist* Table of Contents. Find the article in the table of contents at GSW (ammin.geoscienceworld.org) or MSA (www.minsocam.org), and then click on the deposit link.

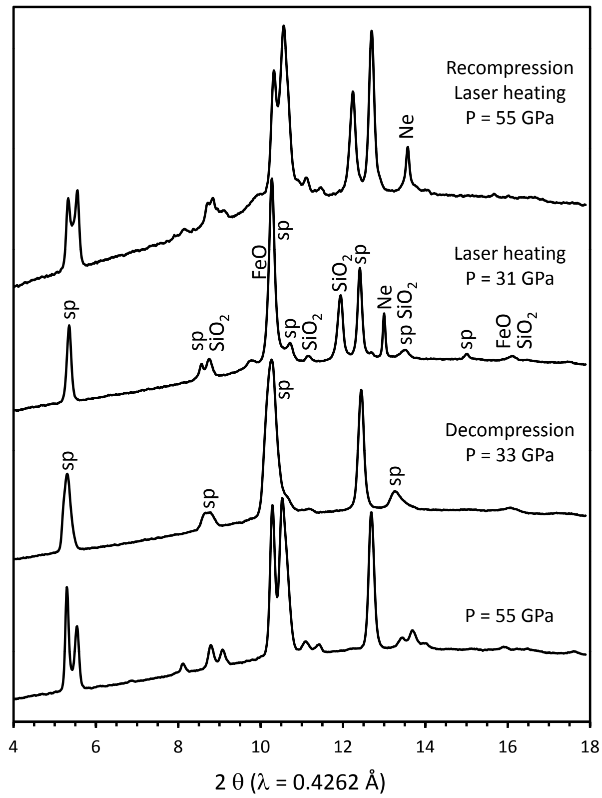

FIGURE 4. The decompression experiment confirms a reversible transition between cubic and orthorhombic phases. Subsequent laser heating at 1500 K and 31 GPa reveals decomposition from spinel to rhombohedral FeO and SiO_2 stishovite.

Si tetrahedra subsidiary changes the coordination to the sixfold octahedron. The Mössbauer spectra of Fe_2SiO_4 taken at 61 GPa by Greenberg et al. (2011) revealed two doublets indicating two independent ferrous sites. The spectra are more consistent with *I*-Fe_2SiO_4 structure than their proposed rhombohedral structure with only one Fe site.

The Si atom changes coordination from fourfold in the spinel phase to sixfold in *I*-Fe_2SiO_4 with site symmetry $2/m$ ($4a$). This change in coordination results in a chain of octahedra parallel to the <100> direction in *I*-Fe_2SiO_4. The octahedral arrays of SiO_6 and FeO_6 octahedra are shown in Figure 8, and the result of the structural refinement of the *I*-Fe_2SiO_4 phase is shown in

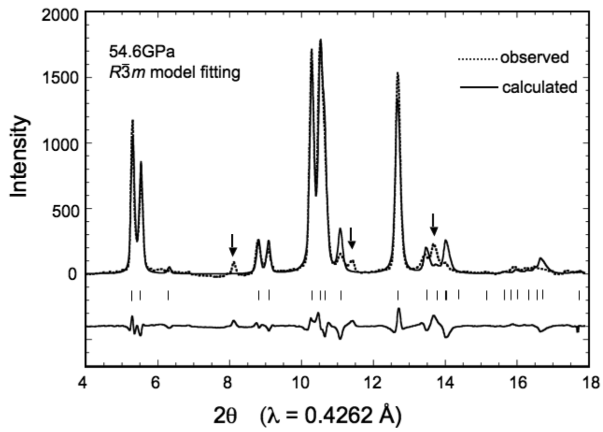

FIGURE 5. Rietveld profile fitting of the initial structure model of rhombohedral Fe_2SiO_4 to the data obtained at 54.6 GPa. The rhombohedral structure model (space group $R\bar{3}m$) is simply derived from a distortion along the <111> direction of the spinel structure. Peaks indicated by the arrows are not indexed.

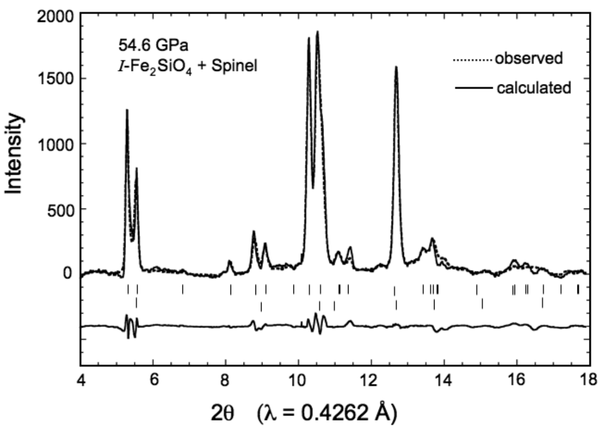

FIGURE 6. Rietveld profile fitting of diffraction data obtained at 54.6 GPa, assuming a two-phase mixture of orthorhombic Fe_2SiO_4 and spinel. Upper and lower vertical bars indicate peak positions for orthorhombic Fe_2SiO_4 and spinel, respectively.

Table 3. The transition is induced by atomic displacements in the spinel structure, which generates the orthorhombic distortion in the I-Fe_2SiO_4 arrangement. The lattice parameters of spinel and I-Fe_2SiO_4 is characterized by the following the axial relation:

$$a_{\text{orth}} = b_{\text{orth}} = d_{\text{spinel }110} = \sqrt{2}/2a_{\text{spinel}}$$

$$c_{\text{orth}} = c_{\text{spinel}}$$

where the subscripts orth represents orthorhombic structure. The structure of I-Fe_2SiO_4 is generated by the a little compression along the <001> direction of the spinel structure and simultaneous elongation along <110> of the spinel direction. This is equivalent to a martensitic transformation with translation vector of $\langle \overrightarrow{1/8}\,\overrightarrow{1/8}\,\overrightarrow{1/8} \rangle$ on each slab in the spinel structure, as illustrated in Figure 9. The density of I-Fe_2SiO_4 at 54.6 GPa is 5.620 g/cm^3, about 1% larger than that of the residual spinel phase 5.572 g/cm^3, as shown in Table 1.

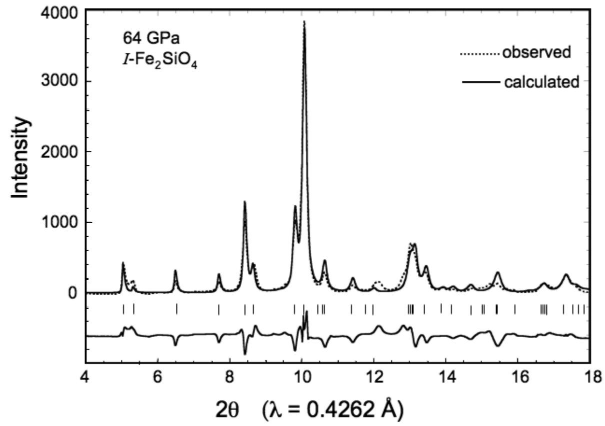

FIGURE 7. Rietveld profile fitting of diffraction data obtained at 64 GPa. Rietveld profile fitting was carried out in consideration of two-phase mixture of I-Fe_2SiO_4 and spinel. No spinel peaks are, however, detected and only a single phase of I-Fe_2SiO_4 is observed. Vertical bars indicate peak positions of the I-Fe_2SiO_4.

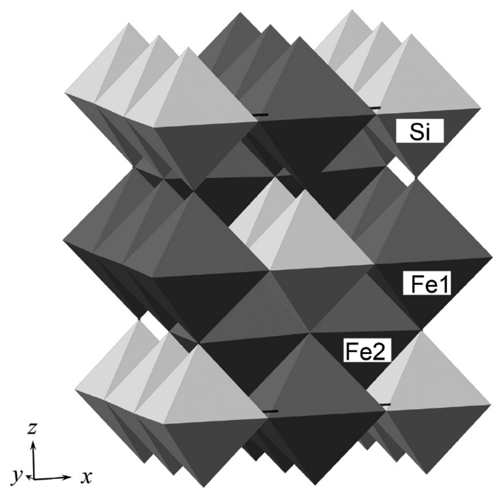

FIGURE 8. There are two distinct octahedral Fe sites, Fe1 and Fe2. Si also is located at the site of octahedral coordination. Fe1 and Fe2 octahedra create layers parallel to the (101) and (011) planes, respectively. SiO_6 octahedra make an array in the direction of <010>.

Spin-state change inducing the structure transition

Photoemission spectroscopy shows that intra-atomic interactions dominate the $K\beta'$ spectral line shape. $K\beta'$ and $K\beta_{1,3}$ lines shift toward each other with decreasing valence spin and (3p, 3d) exchange interaction (Lin et al. 2005, 2007; Li et al. 2006). In previous work, we found a high-spin to intermediate-spin transition in Fe_2TiO_4 at about 19 GPa (Yamanaka et al. 2013). The result and the transition pressure of Fe_3O_4 at 15.8 GPa (Ding et al. 2008) and are much lower spin transition pressures as compared with magnetio-wüstite and other earth materials (Badro et al. 1999; Lin et al. 2005, 2010). X-ray emission (XES) spectra in the Fe$K\beta$ region for the spinel phase of Fe_2SiO_4 are presented in Figure 10, and indicate an intermediate spin state, resulting from the relative integrated intensities due to the energy shift of Fe$K\beta'$.

TABLE 3. Structure parameters of high-pressure phase of *I*-Fe_2SiO_4

Pressure			44.6 GPa[a]	54.6 GPa[a]	64.8 GPa
Space group			*Imma*	*Imma*	*Imma*
Unit molecule			4	4	4
	a (Å)		5.551(3)	5.543(1)	5.522(3)
	b (Å)		6.030(4)	6.032(2)	6.025(4)
	c (Å)		7.241(5)	7,201(4)	7.185(5)
V (Å^3)			242.4(4)	240.8(2)	239.0(2)
	wR_P		2.996	2.531	2.369
	R_p		1.993	1.354	7.573
	R_F		0.985	1.042	4.088
	s		0.4047	0.3436	1.8538
Si	4*a*	*x*	0.0	0.0	0.0
		y	0.0	0.0	0.0
		z	0.0	0.0	0.0
		B_{iso}	4.83(2)	4.87(2)	2.05(2)
Fe1	4*b*	*x*	0.0	0.0	0.0
		y	0.0	0.0	0.0
		z	0.5	0.5	0.5
		B_{iso}	6.74(1)	3.54(1)	2.90(1)
Fe2	4*c*	*x*	0.25	0.25	0.25
		y	0.25	0.25	0.25
		z	0.25	0.25	0.25
		B_{iso}	4.92(1)	3.88(3)	2.92(5)
O1	8*h*	*x*	0.0	0.0	0.0
		y	0.5101(9)	0.5073(5)	0.5068(9)
		z	0.7652(9)	0.7608(8)	0.7610(8)
		B_{iso}	3.6531)	4.00(1)	3.72(2)
O2	8*i*	*x*	0.2371(9)	0.2342(8)	0.2333(2)
		y	0.25	0.25	0.25
		z	0.0022(9)	0.0014(9)	0.0012(6)
		B_{iso}	5.91(2)	6.24(5)	5.54(5)

Notes: Reliability factors for the least-squares calculation are

$$wR_p = \left[\frac{\sum_i w_i\left|y_i - f_i(x)\right|}{\sum_i w_i y_i}\right]^{1/2},\ R_p = \frac{\sum_i\left|y_i - f_i(x)\right|}{\sum_i y_i},$$

$$R_F = \frac{\sum_k\left|F_{k\,\mathrm{obs}}\right| - \left|F_{k\,\mathrm{cal}}\right|}{\sum_k F_{k\,\mathrm{obs}}},\ s = \left[\frac{\sum_i w_i\left|y_i - f_i(x)\right|}{N-P}\right]^{1/2}$$

where *I* and *F* indicate the integrated intensity of the diffraction peak and structure factor, respectively. y_i is the observed diffraction intensity at the i-th position in 2θ, and $f(x)$ is the calculated intensity. *N* and *P* indicate the total number of data points and variable parameters, respectively. The variable *w* is a weight for the data points.
[a] The high-pressure phase coexists with the residual spinel phase.

The integrated absolute difference (IAD) is proportional to the Fe fraction in high-spin state (Vanko et al. 2006). The observed electronic spin transition pressure of *I*-Fe_2SiO_4 starts at about 17 GPa. This is a little lower pressure than the structural transition pressure of 20 GPa observed by XRD. From the high-spin (HS) to intermediate-spin (IS) transition, the $K\beta'$ peak intensity decreases gradually. However, an ideal low-spin state (LS) was not generated even at 65 GPa of the highest pressure achieved in this work. The spin transition starts at a little lower pressure than the structural transition pressure of many iron-bearing oxides and silicates, as observed by X-ray diffraction. For example, XES measurements on Fe_3O_4 by Ding et al. (2008) indicate that the spin transition takes place at a lower pressure (15.8 GPa) than the structural change to the post-spinel phase (23 GPa). Fe_2TiO_4 also undergoes a transition to an intermediate-spin state beginning at 14 GPa (Yamanaka et al. 2013).

DISCUSSION

Pressure-induced electronic spin transitions of ferrous ion are a crucial factor in the compression behavior of spinels, magnesiowüstite, perovskites, and post-perovskites. A high-spin to intermediate-spin transition of Fe_3O_4 occurs at 15.8 GPa (Ding et al. 2008) and Fe_2TiO_4 at about 19 GPa (Yamanaka et al. 2013). Those pressures are a little lower than structure transition pressure. The change in the spin state of Fe_2SiO_4 observed at ~17 GPa should also have a significant effect on the effective ionic radii. In the high-spin state of Fe^{2+} ($3d^6$) occupying the octahedral site at ambient conditions, two electrons reside in the doubly degenerate e_g orbital set and four in the triply degenerate t_{2g} orbital set. In the low-spin state under high-pressure conditions, one or two e_g electrons move down in energy to the t_{2g} orbital set, which opens up additional possibilities for *d-p-*π bonding (Fe t_{2g}–O 2*p*), but less possibilities for σ-type (Fe e_g–O 2*p*) bonding. These ligand configuration effects combine to give a smaller effective ionic radius for the low-spin state of Fe^{2+}. In the case of Fe_3O_4, the XES result can be interpreted as the spin transition at Fe^{2+} in the octahedral site, while the two Fe^{3+} remain in the high-spin state.

The ionic radii reported by Shannon (1976) gives the radii for Fe^{2+} as 0.780 Å at HS and 0.61 Å at LS. The spin transition therefore reduces the ferrous ion radius by about 20%. The Fe^{2+}-O bond distance is likewise reduced from 2.16 to 1.99 Å (given the oxygen ion radius of 1.38 Å). A change in the effective ionic radius brings about a polyhedral distortion. While the Si-O bond is not easily compressed, the Fe-O bond length is reduced dramatically under compression. The observed decrease in the lattice parameter leads to the corresponding change in octahedral volume. The volume ratio of the octahedron shows a distinct change due to the compression behavior of Fe-O bond distance at 20 GPa. These discontinuous changes are induced by the spin transition, starting at 17 GPa. However, the volume of the tetrahedron does not show a noticeable change in contrast to the octahedra. Fe2 ion changes the spin state to an intermediate spin, resulting in its greater distortion of FeO_6 and smaller bond lengths, but Fe1 ion located at a larger and less distorted site probably remains in the HS state even at 64 GPa (Table 4).

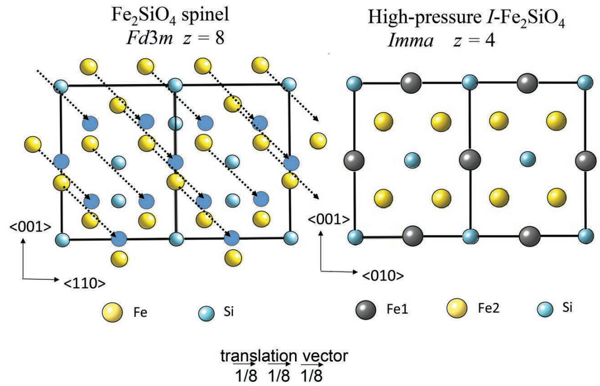

FIGURE 9. Fe_2SiO_4 spinel (ringwoodite ahrensite) and high-pressure phase *I*-Fe_2SiO_4 are presented in the **left** and **right** figure, respectively. Arrow indicates a martensitic transformation with translation vector <$\overrightarrow{1/8}$ $\overrightarrow{1/8}$ $\overrightarrow{1/8}$>, which generates the *I*-Fe_2SiO_4 structure from the spinel. The shadowed circles in the **left** figure represent the atomic positions of *I*-Fe_2SiO_4. (Color online.)

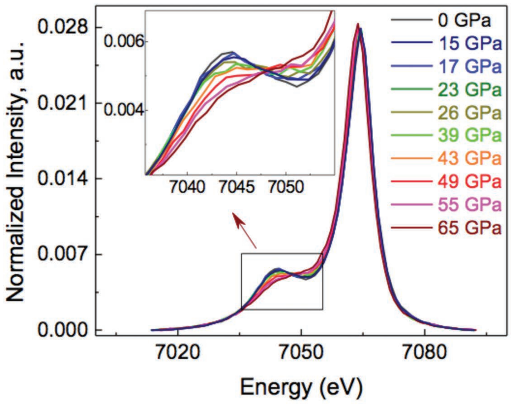

FIGURE 10. Fe*K*β X-ray emission spectra with increasing pressure up to 64.8 GPa. The inset shows the expanded *K*β′ spectra, indicating an intermediate spin transition. The spin transition occurs at ~17 GPa. (Color online.)

IMPLICATIONS

Numerous investigations of the structure transitions and decompositions of spinels have been executed under extreme conditions. Silicate spinels with transition elements or mixed-charge cations have been intensively studied from various viewpoints such as their magnetic susceptibility, electric conductivity, or elastic property.

The olivine-spinel transformation has been strongly studied for significance at the transition zone of the Earth's mantle. Fe_2SiO_4 has an olivine structure (α-Fe_2SiO_4, fayalite) at ambient conditions and transforms directly into spinel (γ-Fe_2SiO_4, ahrensite) under high pressure at ambient temperature. Silicate spinels have been known as an essentially metastable phase at ambient conditions.

There are several passes of spinel structure transformations. Some oxide spinels with transition elements have their high-pressure polymorphs due to the transition without decomposition. A pseudo-rhombohedral phase at pressures above 30 GPa and ambient temperature was reported on the basis of powder diffraction data and Mössbauer data (Greenberg et al. 2011). However, structure parameters including atomic positional parameters of the high-pressure phase are not reported in their paper and their Rietveld analysis at 48(2) GPa did not consider the residual spinel phase in the refinement. Hence, several peaks are not clearly fitted.

TABLE 4. Deformation of Si, Fe1, and Fe2 octahedra of *I*-Fe_2SiO_4

Pressure			44.6 GPa	54.6 GPa	64.8 GPa
Si	O1 x2	(Å)	1.775(4)	1.723(4)	1.718(4)
	O2 x4	(Å)	2.001(4)	1.990(4)	1.982(4)
	mean	(Å)	1.901(4)	1.901(4)	1.894(4)
	volume	(Å³)	8.99(6)	8.99(6)	8.89(4)
Fe1	O1 x2	(Å)	1.921(5)	1.879(3)	1.876(3)
	O2 x4	(Å)	2.098(5)	2.108(3)	2.107(3)
	mean	(Å)	2.039(5)	2.032(3)	2.030(3)
	volume	(Å³)	11.26(6)	11.13(5)	11.09(5)
Fe2	O1 x4	(Å)	2.008(6)	2.017(6)	2.015(4)
	O2 x2	(Å)	1.796(6)	1.792(6)	1.790(4)
	mean	(Å)	1.937(6)	1.942(8)	1.940(4)
	volume	(Å³)	9.58(4)	9.66(2)	9.61(2)

Note: Deformation of each octahedron is different with pressure.

This paper shows a structural change in Fe_2SiO_4 spinel under high pressure up to 64 GPa. A new high-pressure structure of *I*-Fe_2SiO_4 is determined by Rietveld profile fitting of synchrotron X-ray diffraction data at ambient temperature. A transition from the cubic spinel structure to a body centered orthorhombic phase (*I*-Fe_2SiO_4) with space group *Imma* and $Z = 4$ was first observed at approximately 39 GPa. The structure of *I*-Fe_2SiO_4 has two crystallographically distinct FeO_6 octahedral sites and Si atom changes its configuration.

In addition to the new structure, we first found two different compression curves of the lattice parameter in the spinel phase and the discontinuity at ~20 GPa. Fe*K*β X-ray emission measurements at elevating pressure show that the transition from high-spin (HS) state to intermediate-spin (IS) state begins at 17 GPa in the spinel phase. The IS electronic state is gradually enhanced with pressure, which generates an isostructural change in the lattice parameter at 20 GPa. The spin transition induces the compression of the bond length, resulting in the structure transition at 39 GPa. The spin transition can be emphasized for the trigger of the structure transition.

ACKNOWLEDGMENTS

We express our great thanks to E. Ito of Okayama University, Japan, for providing us Fe_2SiO_4 spinel samples. This work was sponsored by the Carnegie/DOE Alliance Center (CDAC, DE-FC52-08NA28554). Support from DOE-BES (DE-FG02-06ER46280) Energy Frontier Research Center funded by the U.S. Department of Energy (DOE), Office of Science. The present investigation was also performed under the auspices of KEK proposal no. 2004G229 for powder diffraction at BL-13A and BL-18C of the Photon Factory, Tsukuba, Japan.

REFERENCES CITED

Akimoto, S., and Fujisawa, H. (1967) Olivine-spinel solid solution equilibria in the system Mg_2SiO_4-Fe_2SiO_4. Journal of Geophysical Research, 73, 1467–1479.
Armentrout, M., and Kavner, A. (2011) High pressure, high temperature equation of state for Fe_2SiO_4 ringwoodite and implications for the Earth's transition zone. Geophysical Research Letters, 38, L08309.
Badro, J., Struzhkin, V.V., Shu, J., Hemley, R.J., Mao, H.K., Kao, C.C., Rueff, J.P., and Shen G. (1999) Magnetism in FeO at megabar pressures from X-ray emission spectroscopy. Physical Review Letters, 83, 4101–4104.
Bassett, W.A., and Ming, L.C. (1972) Disproportionation of Fe_2SiO_4 to 2FeO + SiO_2 at pressures up to 250 kbar and temperatures up to 3000 °C. Physics of the Earth and Planetary Interiors, 6, 154–160.
Birch, F. (1947) Finite elastic strain of cubic crystals. Physical Review, 71, 809–824.
Boultif, A., and Louer, D. (2004) Powder pattern indexing with the dichotomy method. Journal of Applied Crystallography, 37, 724–731.
Burnley, P.C., Green, H.W., and Prior, D. (1991) Faulting associated with the olivine to spinel transformation in Mg_2GeO_4 and its implications for deep-focus earthquakes. Journal of Geophysical Research, B96, 425–443.
Derzsi, M. Piekarz, P., Tokár, K., Jochym, P.T., Łaewski, J., Sternik, M., and Parlinski, K. (2011) Comparative *ab initio* study of lattice dynamics and thermodynamics of Fe_2SiO_4- and Mg_2SiO_4-spinels. Journal of Physics: Condensed Matter, 23, 105401.
Ding, Y., Haskel, D., Ovchinnikov, S.G., Tseng, Y.C., Orlov, Y.S., Lang, J.C., and Mao, H.K. (2008) Novel pressure-induced magnetic transition in magnetite (Fe_3O_4). Phyical Review Letters, 100, 045508.
Fei, Y., Mao, H,K., and Mysen, B.O. (1991) Experimental determination of element partitioning and calculation of phase relations in the MgO-FeO-SiO_2 system at high pressure and high temperature. Journal Geophysical Research, B96, 2157–2169.
Fei, Y., Mao, H.K., Hemley, R.J., Shu, J.F., and Shen, G. (1999) In situ structure determination of the high-pressure phase of Fe_3O_4. American Mineralogist, 84, 203–206.
Greenberg, E., Dubrovinsky, L.S., McCammon, C., Rouquette, J., Kantor, I., Prakapenka,V., Rozenberg, G.K., and Pasternak, M. (2011) Pressure-induced structural phase transition of the iron end-member of ringwoodite (γ-Fe_2SiO_4) investigated by X-ray diffraction and Mössbauer spectroscopy. American Mineralogist, 96, 833–840.
Hazen, R.M. (1993) Comparative compressibilities of silicate spinels: Anomalous behavior of $(Mg,Fe)SiO_3$. Science, 259, 206–209.
Irifune, T., Nishiyama, N., Kuroda, K., Inoue, T., Isshiki, M., Utsumi, W., Funakoshi, K., Urakawa, S., Uchida, T., and Katsura, T. (1998) Postspinel phase

boundary in Mg_2SiO_4 determined by in situ X-ray diffraction. Science, 279, 1698–1700.
Ito, E., and Takahashi, E. (1987) Melting of peridotite under the lower mantle condition. Nature, 328, 514–517.
——— (1989) Postspinel transformations in the system Mg_2SiO_4-Fe_2SiO_4 and some geophysical implications. Journal of Geophysical Research, 94, 10637–10646.
Izumi, F., and Ikeda, T. (2000) A Rietveld-analysis program RIETAN-98 and its applications to zeolites. European Powder Diffraction. Materials Science Forum, 198–203.
Katsura, T., and Ito, E. (1989) The system Mg_2SiO_4-Fe_2SiO_4 at high pressure and temperature: Precise determination of stabilities of olivine, modified spinel and spinel. Journal of Geophysical Research, 94, 15,663–15,670.
Kiefer, B., Stixrude, L., and Wentzcovitch, R.M. (1997) Calculated elastic properties and anisotropy of Mg_2SiO_4 spinel at high pressure. Geophysical Research Letters, 24, 2841–2844.
Kontny, A., Woodland, A.B., and Koch, M. (2004) Temperature-dependent magnetic susceptibility behavior of spinelloid and spinel solid solutions in the systems Fe_2SiO_4–Fe_3O_4 and $(Fe,Mg)_2SiO_4$–Fe_3O_4. Physics and Chemistry of Minerals, 31, 28-40.
Leven, J.H., Jackson, I., and Ringwood, A.E. (1981) Upper mantle seismic anisotropy and lithospheric decoupling. Nature, 289, 234–239.
Li, J., Struzhkin, V.V., Mao, H.K., Shu J., Hemley, R.J., Fei, Y., Mysen, B., Dera, P., Prakapenka, V., and Shen, G. (2004) Electronic spin state of iron in lower mantle perovskite. Proceedings of the National Academy of Sciences, 101, 14027–14030.
Li, J., Sturhahn, W., Jackson, J., Struzhkin, V.V., Lin J.F., Mao, H.K., and Shen, G. (2006) Pressure effect on the electronic structure of iron in $(Mg,Fe)(Si,Al)O_3$ perovskite: A combined synchrotron Mössbauer and X-ray emission spectroscopy study up to 100 GPa. Physics and Chemistry of Minerals, 33, 575–585.
Li, L., Cares, P., and Weidner, D.J. (2007) Effect of cation ordering and pressure on spinel elasticity by *ab initio* simulation. American Mineralogist, 92, 174–178.
Lin, J.F., Struzhkin, V.V., Jacobsen, S.D., Shen, G., Prakapenka,V.B., Mao, H.K., and Hemley, R.J. (2005) Spin transition of iron in magnesiowüstite in the Earth's lower mantle. Nature, 436, 377–380.
Lin, J.F., Struzhkin, V.V., Jacobsen, S.D., Hu, M.Y., Chow, P., Kung, J., Liu, H., Mao, H.K., and Hemley, R.J. (2007) X-ray emission spectroscopy with a laser-heated diamond anvil cell: A new experimental probe of the spin state of iron in the Earth's interior. Journal of Synchrotron Radiation, 12, 637–641.
Lin, J.F., Mao, Z., Jarrige, I., Xiao,Y.M., Chow, P., Okuchi, T., Hiraoka, N., and Jacobsen, S.D. (2010) Resonant X-ray emission study of the lower-mantle ferropericlase at high pressures. American Mineralogist, 95, 1125–1131.
Liu, Q., Liu, W., Whitaker, M.L., Wang, L., and Li, B. (2008) Compressional and shear wave velocities of Fe_2SiO_4 spinel at high pressure and high temperature. High Pressure Research, 28, 405–413.
Ma, C.B. (1975) Structure refinement of high-pressure Ni_2SiO_4 spinel. Zeitshrift für Kristallographie, 141, 126–137.
Madon, M., and Poirier, J.P. (1983) Transmission electron microscopic observation of α, β and γ $(Mg, Fe)_2SiO_4$ in shocked meteorite: Planar defects and polymorphic transitions. Physics of the Earth and Planetary Interiors, 33, 31–44.
Mao, H.K., Xu, J., and Bell, P.M. (1986) Calibration of the ruby pressure gauge to 800-kbar under quasi-hydrostatic conditions. Journal Geophysical Research, 91, 4673–4676.
Marumo, F., Isobe, M., Saito, Y., Yagi, T., and Akimoto, S. (1974) Electron-density distribution in crystals of g-Ni_2SiO_4. Acta Crystallographica, B30, 1904–1906.
Marumo, F., Isobe, M., and Akimoto, S. (1977) Electron-density distribution in crystals of γ-Fe_2SiO_4 and γ-Co_2SiO_4. Acta Crystallographica, B33, 713–716.
Matsuzaka, K., Akaogi, M., Suzuki, T., and Suda, T. (2000) Mg-Fe partitioning between silicate spinel and magnesiowüstite at high pressure: experimental determination and calculation of phase relations in the system Mg_2SiO_4-Fe_2SiO_4. Physics and Chemistry of Minerals, 27, 310–319.
Mattila, A., Rueff, J.P., Badro, J., Vankó, G., Shukla, A., (2007) Metal-ligand interplay in strongly correlated oxides: a parameterized phase diagram for pressure-induced spin transitions. Physical Review Letters, 98, 196404.
Morimoto, N., Akimoto, S., Koto, K., and Tokonami, M. (1970) Crystal structures of high-pressure modifications of Mn_2GeO_4 and Co_2SiO_4. Physics of the Earth and Planetary Interiors, 3,161–165.
Morimoto, N., Tokonami, M., Watanabe, M., and Koto, K. (1974) Crystal structures of three polymorphs of Co_2SiO_4. American Mineralogist, 59, 475–485.
Nestola, F., Balić-Žunić, T., Koch-Müller, M., Secco, L., Princivalle, F., Parisi, F., and Dal Negro, A. (2011) High-pressure crystal structure investigation of synthetic Fe_2SiO_4 spinel. Mineralogical Magazine, 75, 2649–2655.
Ohtaka, O., Tobe, H., and Yamanaka, T. (1997) Phase equillibria for the Fe_2SiO_4±Fe_3O_4 system under high pressure. Physics and Chemistry of Minerals, 24, 555–560.
Piermarini, G.J., Blook, S., Barnett, J.D., and Forman, R.A. (1975) Calibration of the pressure dependence of the R1 ruby fluorescence line to 195 kbar. Journal of Applied Physics, 46, 2774–2780.
Price, G.D., Putnis, A., and Smith D.G.W. (1982) A mechanism for the spinel to b phase transformation in $(Mg,Fe)_2SiO_4$ system. Nature, 296, 729–731.
Ringwood, A.E., and Irifune, T. (1988) Nature of the 650-km seismic discontinuity: implications for mantle dynamics and differentiation. Nature, 331, 131–136.
Shannon, R.D. (1976) Revised effective ionic radii and systematics of interatomic distances in halides and chalcogenides. Acta Crystallographica, A32, 751–767.
Shim, S-H., Duffy, T.S., and Shen, G. (2001) The post-spinel transformation in Mg_2SiO_4 and its relation to the 660-km seismic discontinuity. Nature, 411, 571–574, http://dx.doi.org/10.1038/35079053.
Vanko, G., Neisius, T., Molnár, G., Renz, F., Kárpáti, S., Shukla, A., and de Groot, F.M.F. (2006) Probing the 3d spin momentum with X-ray emission spectroscopy: The case of molecular-spin transitions. Journal of Physical Chemistry B, 110, 11647–11653.
Woodland, A.B., and Angel, R.J. (2000) Phase relations in the system fayalite-magnetite at high pressures and temperatures. Contributions to Mineralogy and Petrology, 139, 734–747.
Woodland, A., Schollenbruch, K., Frost, D., and Langenhorst, F. (2010) The post-spinel transition in Fe_3O_4-Fe_2SiO_4 and Fe_3O_4-$FeCr_2O_4$ solid solutions. Geophysical Research Abstracts, 12, EGU2010-12685.
Xu, Y., Poe, B.T., Shankland, T.J., and Rubie, D.C. (1998) Electrical conductivity of olivine, wadsleyite, and ringwoodite under upper-mantle conditions. Science, 280, 1415–1418.
Yagi, T., Marumo, F., and Akimoto, S. (1974) Crystal structures of Fe_2SiO_4 and Ni_2SiO_4. American Mineralogist, 59, 486–490.
Yagi, T., Akaogi, M., Shimomura, O., Suzuki, T., and Akimoto, S. (1987) In situ observation of the olivine-spinel phase transformation in Fe_2SiO_4 using synchrotron radiation. Journal of Geophysical Research, 92, 6207–6213.
Yamanaka, T., and Okita, M. (2001) Magnetic properties of the Fe_2SiO_4-Fe_3O_4 spinel solid solution. Physics and Chemistry of Minerals, 28, 102–109.
Yamanaka, T., Shimazu, H., and Ohta, K. (2001) Electric conductivity of the Fe_2SiO_4-Fe_3O_4 spinel solid solution. Physics and Chemistry of Minerals, 28, 110–118.
Yamanaka, T., Kyono, A., Nakamoto, Y., Meng, Y., Kharlamova, S., Struzhkin, V.V., and Mao, H.K. (2013) High-pressure phase transitions of $Fe_{3-x}Ti_xO_4$ solid solution up to 60 GPa correlated with electronic spin transition. American Mineralogist, 98, 736–744.

MANUSCRIPT RECEIVED SEPTEMBER 13, 2013
MANUSCRIPT ACCEPTED JANUARY 20, 2015
MANUSCRIPT HANDLED BY KRISTINA LILOVA